

# Magnetic properties and pairing tendencies of the iron-based superconducting ladder $\text{BaFe}_2\text{S}_3$ : Combined *ab initio* and density matrix renormalization group study

Niravkumar D. Patel,<sup>1,2</sup> Alberto Nocera,<sup>3</sup> Gonzalo Alvarez,<sup>3</sup> Ryotaro Arita,<sup>4,5</sup> Adriana Moreo,<sup>1,2</sup> and Elbio Dagotto<sup>1,2</sup>

<sup>1</sup>*Department of Physics and Astronomy, The University of Tennessee, Knoxville, Tennessee 37996, USA*

<sup>2</sup>*Materials Science and Technology Division, Oak Ridge National Laboratory, Oak Ridge, Tennessee 37831, USA*

<sup>3</sup>*Computer Science & Mathematics Division and Center for Nanophase Materials Sciences, Oak Ridge National Laboratory, Oak Ridge, Tennessee 37831, USA*

<sup>4</sup>*JST, ERATO, Isobe Degenerate  $\pi$ -Integration Project, Aoba-ku, Sendai 980-8577, Japan*

<sup>5</sup>*RIKEN Center for Emergent Matter Science, Wako, Saitama 351-098, Japan*

(Received 3 April 2016; revised manuscript received 16 June 2016; published 10 August 2016)

The recent discovery of superconductivity under high pressure in the two-leg ladder compound  $\text{BaFe}_2\text{S}_3$  [H. Takahashi *et al.*, *Nat. Mater.* **14**, 1008 (2015)] opens a broad avenue of research, because it represents the first report of pairing tendencies in a quasi-one-dimensional iron-based high-critical-temperature superconductor. Similarly, as in the case of the cuprates, ladders and chains can be far more accurately studied using many-body techniques and model Hamiltonians than their layered counterparts, particularly if several orbitals are active. In this publication, we derive a two-orbital Hubbard model from first principles that describes individual ladders of  $\text{BaFe}_2\text{S}_3$ . The model is studied with the density matrix renormalization group. These first reported results are exciting for two reasons: (i) at half-filling, ferromagnetic order emerges as the dominant magnetic pattern along the rungs of the ladder, and antiferromagnetic order along the legs, in excellent agreement with neutron experiments; and (ii) with hole doping, pairs form in the strong coupling regime, as found by studying the binding energy of two holes doped on the half-filled system. In addition, orbital selective Mott phase characteristics develop with doping, with only one Wannier orbital receiving the hole carriers while the other remains half-filled. These results suggest that the analysis of models for iron-based two-leg ladders could clarify the origin of pairing tendencies and other exotic properties of iron-based high-critical-temperature superconductors in general.

DOI: [10.1103/PhysRevB.94.075119](https://doi.org/10.1103/PhysRevB.94.075119)

## I. INTRODUCTION

The understanding of the high-critical-temperature ( $T_c$ ) superconductors based on iron continues attracting the attention of the condensed matter community [1–7]. It is widely believed that these studies may not only have potential technological applications, but they may also shed light on other high- $T_c$  superconductors such as those based on copper. While early theoretical studies of the iron-based compounds were guided by simple Fermi surface nesting ideas that may have captured important properties of these materials such as the symmetry of the superconducting state, more recent investigations are increasingly suggesting that the effect of Coulombic repulsion between electrons cannot be neglected [6]. For example, there are compounds that are superconducting but do not have hole pockets, and thus no nesting effects, at the Fermi surface [8]. There are also materials with robust magnetic local moments even at room temperature [9,10], in disagreement with weak coupling perspectives where the formation of moments and their long-range order occur simultaneously upon cooling. Moreover, complex spin arrangements have been unveiled in several materials, as recently reviewed [7]. All these results suggest that repulsive interactions between electrons are important to fully understand these compounds' properties. However, the theoretical analysis of multiorbital Hubbard models is challenging because of the absence of reliable many-body tools to study their properties in layered systems. In particular, thus far the only theoretical evidence that superconductivity can be induced in these compounds via antiferromagnetic (AFM) fluctuations relies exclusively on BCS gap equations and random phase approximation

techniques. Can we generate more robust theoretical evidence for AFM-based superconductivity in these compounds?

In the context of the copper-oxide high- $T_c$  superconductors, finding crystal structures simpler than layers but still with intriguing quantum mechanical many-body properties proved to be a fruitful path for progress in that field. One of the reasons is that theorists can perform model Hamiltonian calculations with more accuracy in, e.g., quasi-one-dimensional systems. In fact, spin-1/2 Cu-oxide two-leg ladders have been much studied in cuprates because of their unusual spin gap, induced by the ladder geometry [11–13]. The Cu-oxide-ladder spin state is dominated by rung spin-singlets, and it was theoretically predicted that such a system should have a tendency to superconductivity upon doping. This was verified in high-pressure experiments at  $\sim 3$  GPa for the case of  $\text{Sr}_{0.4}\text{Ca}_{13.6}\text{Cu}_{24}\text{O}_{41.84}$ , reporting a critical temperature of 12 K [14]. Due to its quasi-one-dimensional character, it was possible to employ a variety of accurate many-body techniques for ladders, showing agreement between theoretical predictions and experimental results, an agreement that has provided considerable support to the notion that superconductivity in cuprates originates in AFM fluctuations.

These important earlier results in the context of copper-oxide ladders suggest that progress in the understanding of iron-based superconductors would be possible if similar quasi-one-dimensional structures could be prepared and theoretically studied. For this reason considerable interest was generated by recent studies of  $\text{BaFe}_2\text{S}_3$  because this material contains double chains made of  $[\text{Fe}_2\text{S}_3]^{2-}$  blocks separated by Ba [15–23]. The resulting structure contains two extended Fe-Fe directions (the “legs”) connected by Fe-Fe bonds of similar

strength (the “rungs”) thus defining two-leg ladders very similar to those in the cuprates. A difference is that the Cu-Cu bridge in the cuprates’ ladders is made by an oxygen in between the coppers, while in chalcogenides the bridges between irons are provided by selenium, which is located up and down the middle of the iron plaquettes. Thus, as in their two-dimensional counterparts, electronic hoppings of similar strength are to be expected for the chalcogenides not only along legs and rungs, but also along the plaquette diagonals.

BaFe<sub>2</sub>Se<sub>3</sub> is an insulator, with an activation energy between 0.13 eV [18] and 0.178 eV [16], long-range AFM order at  $\sim 250$  K induced by weak residual interladder interactions, and low-temperature magnetic moments  $\sim 2.8 \mu_B$  [15–17]. Remarkably, neutron diffraction studies reported a dominant magnetic order at low temperature involving blocks of four iron atoms with their moments aligned, coupled antiferromagnetically along the ladder direction [15,18]. When K replaces Ba, thus leading to KFe<sub>2</sub>Se<sub>3</sub>, the magnetic state changes to an arrangement where the spins in the same rung are coupled ferromagnetically but they are antiferromagnetically ordered in the long-ladder direction [19]. Theoretical studies primarily employing the Hartree Fock approximation [21] unveiled a rich phase diagram for two-leg ladder multiorbital Hubbard models, with a plethora of phases including both states already found in the Ba- and K-based ladders as well as several other competitors. These exotic spin arrangements arise from frustrating tendencies between the staggered AFM state that dominates at small Hund coupling and the ferromagnetic (FM) state stable at large Hund coupling [21]. Hartree-Fock results for layers [24] and chains [25] also suggest a complex landscape of competing magnetic states in those geometries.

Recently, an unexpected experimental result has been reported using BaFe<sub>2</sub>S<sub>3</sub> [26,27], where S replaces Se but keeps the two-leg ladder structure the same. This material was found to become superconducting at a pressure above 10 GPa with an optimal critical temperature  $T_c = 24$  K. The parent compound, i.e., the same material but at ambient pressure, is a Mott insulator with the same magnetic order as KFe<sub>2</sub>Se<sub>3</sub> namely involving FM rung and AFM leg spin correlations with a critical temperature  $\sim 120$  K, according to power neutron diffraction studies [26]. These discoveries unveiled the first iron-based superconductor that does not rely on a square lattice structure of irons, opening an intriguing avenue of research similar to the one opened with the discovery of superconductivity in Cu oxide ladders in the context of the cuprates.

The present publication introduces a two-orbital Hubbard model for a two-leg ladder of BaFe<sub>2</sub>S<sub>3</sub>, based on *ab initio* calculations. This model is subsequently solved computationally using the density matrix renormalization group (DMRG) technique [28]. Our main results are two folded. First, we show that at half-filling with two electrons per iron, and using clusters as large as  $16 \times 2$ , there is a robust evidence for the same magnetic order found experimentally involving FM rungs and AFM leg correlations. This magnetic state becomes robust at intermediate and strong Hubbard couplings, in agreement with the growing perception that these materials are not in the weak coupling regime. Second, we assume that in the experiments [26] the high pressure alters the band structure in such a manner that the individual ladders become hole doped,

although the insulator-superconductor transition could also be bandwidth-controlled [26]. In the Cu-oxide based ladders studied some years ago, experiments showed [29] that indeed pressure alters the amount of mobile electrons residing in the two-leg ladders in such a manner that the superconducting state is reached effectively by hole doping of the ladders. Here we simply assume that a similar physics occurs in the iron-based ladders and focus on their hole doping. In fact, studying the cases of one, two, and four holes we have found pairing tendencies when using an  $8 \times 2$  cluster in the strong coupling regime  $U/W \simeq 2$ ,  $W$  being the tight-binding electronic bandwidth. The complexity of the Hamiltonian with two active orbitals and a tight-binding term that must include plaquette diagonal hoppings renders the DMRG calculation so computing time demanding that a confirmation of the pairing tendency beyond  $8 \times 2$  is not possible at present with the DMRG technique and our available computer resources. Nevertheless, the pairing indications we have observed are promising and suggestive that the theoretical study of iron-based two-leg ladders may illuminate the understanding of iron-based superconductors using many-body techniques beyond the diagrammatic random phase approximation.

The organization of the manuscript is as follows. Section II provides details of the *ab initio* calculations. Section III contains the actual model used, many-body technique, and observables studied. Section IV presents our main results, organized separately for zero, one, and two holes, the latter including binding energies. Finally, Sec. V contains our main conclusions.

## II. AB INITIO CALCULATIONS

This section presents the details of the derivation of the multiorbital Hubbard model for the BaFe<sub>2</sub>S<sub>3</sub> ladder from first principles, to be used later in Secs. III and IV. Following the procedure described in Ref. [30], first, a calculation is performed based on the generalized gradient approximation with the QUANTUM ESPRESSO package [31]. There we employed the exchange-correlation functional proposed by Perdew, Burke, and Ernzerhof [32], a plane-wave basis set with a cutoff energy of 40 Ry, and an  $8 \times 8 \times 8$   $\mathbf{k}$  mesh for the first Brillouin zone (BZ). As for the lattice constants, we used the experimental values  $a = 8.78$  Å,  $b = 11.23$  Å, and  $c = 5.29$  Å for the ambient pressure case and reduced them by 4.0%, 8.0%, and 3.4%, respectively, for pressure  $P = 12.4$  GPa [33]. The space group of the system is *Cmcm*, and the atomic positions of Ba(4c), Fe(8e), S(4c), and S(8g) are (0.0, 0.686, 0.25), (0.154, 0.0, 0.0), (0.0, 0.116, 0.25), and (0.208, 0.378, 0.25), respectively [33]. Because the magnetic properties will be considered when we solve the effective two-orbital Hubbard model in the following sections, magnetism was not included in the derivation of the model from first principles [34].

After this initial setup, we constructed two Wannier functions for each Fe atom in the unit cell using the WANNIER90 package [35]. One resulting Wannier orbital mainly consists of the standard  $d_{x^2-y^2}$  orbitals (orbital *a* below), while the other one is primarily made from the standard  $d_{xz}$  orbital (orbital *b* below). The two Wannier orbitals employed here do not have a high symmetry, because the  $d_{x^2-y^2}$  or  $d_{xz}$  orbitals significantly hybridize with other *d*-orbitals or *s-p* orbitals. In particular, for

the latter Wannier orbital there is a substantial contribution of the canonical  $d_{xy}$  orbital. To construct explicitly these orbitals, we have to disentangle their complicated electronic structure. In order to preserve accurately the properties of the low-energy band dispersion, we introduced a “frozen” energy window [36] as large as  $(-0.3 \text{ eV}, 0.2 \text{ eV})$  with respect to  $E_F$ , on top of the ordinary “global” energy window  $(-1.2 \text{ eV}, 1.5 \text{ eV})$ .

After we constructed an eight-band model, we further simplified this model by unfolding the BZ along the  $k_z$  direction. Namely, by introducing a local gauge transformation for one of the two Wannier orbitals to change its sign, we can expand the band dispersion from  $\Gamma$  to  $Z$  in the original BZ, and construct a four-band model [30].

Finally, we want to derive an effective ladder model from the four-band model, namely we wish to arrive to a model restricted to a two-leg ladder. One possibility is to neglect all interladder electron hopping transfers and just focus on the intraladder transfers. However, the bandwidth in the  $k_x$ - $k_y$  plane is not necessarily small (as large as 500 meV at maximum). Thus, in the present study, the effect of interladder transfers is taken into account by considering their average, i.e., we construct our ladder model from the four-band Hamiltonian by considering the case  $k_x = k_y = 0$ .

### III. MODEL AND METHOD

This section explicitly provides the multiorbital Hubbard model derived by the procedure explained before, while Sec. IV will present the magnetic properties and pairing tendencies of  $\text{BaFe}_2\text{S}_3$ . The model studied here breaks up into kinetic energy and interaction terms:  $H = H_K + H_{\text{int}}$ . The tight-binding kinetic energy portion is

$$H_K = \sum_{\substack{i\sigma \\ \gamma\gamma'\alpha}} t_{\gamma\gamma'}^{\alpha} (c_{i\sigma\gamma}^{\dagger} c_{i+\alpha\sigma\gamma'} + \text{H.c.}) + \sum_{i\gamma\sigma} \Delta_{\gamma} n_{i\gamma\sigma}, \quad (1)$$

where the first term represents the hopping of an electron from site  $i$  of a two-leg ladder and orbital  $\gamma$  to site  $i + \vec{\alpha}$  and orbital  $\gamma'$ . The vector  $\vec{\alpha}$  indicates the many different directions possible for the electronic hopping, as shown in the ladder sketch Fig. 1. We use a two-orbital model where we label the

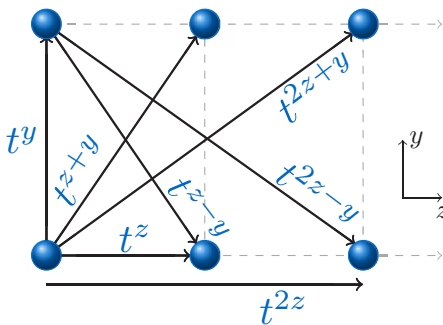


FIG. 1. Schematic representation of the directions of electronic hopping for the two-leg ladder model considered here. The legs of the ladder are arranged in the  $z$  direction, while the rungs are in the  $y$  direction. The hoppings to next-nearest neighbor rungs (i.e.,  $t^{2z}$ ,  $t^{2z-y}$ , and  $t^{2z+y}$ ) are dubbed the “long-range hoppings.” In total, there are seven different hopping directions shown.

downfolded [30] orbitals as  $a$  and  $b$  (i.e.,  $\gamma$  and  $\gamma'$  are restricted to  $a$  and  $b$ ).  $\Delta_{\gamma}$  represents the crystal-field splitting of orbital  $\gamma$ . There are two sets of hopping parameters obtained from fitting the *ab initio* downfolded band structure calculations at different pressures. The crystal fields at  $P = 0.0 \text{ GPa}$  are  $\Delta_a = 0.308$  and  $\Delta_b = -0.229$  (eV units used from now on) while the associated hopping amplitudes are

$$\begin{aligned} t^z &= \begin{bmatrix} -0.215 & -0.149 \\ +0.149 & +0.153 \end{bmatrix}, \\ t^y &= \begin{bmatrix} -0.012 & 0.000 \\ 0.000 & +0.153 \end{bmatrix}, \\ t^{z+y} = t^{z-y} &= \begin{bmatrix} +0.075 & +0.174 \\ -0.174 & +0.083 \end{bmatrix}, \\ t^{2z} &= \begin{bmatrix} -0.137 & +0.004 \\ -0.004 & +0.037 \end{bmatrix}, \\ t^{2z+y} = t^{2z-y} &= \begin{bmatrix} -0.007 & +0.016 \\ -0.016 & -0.041 \end{bmatrix}, \end{aligned} \quad (2)$$

while the crystal fields at  $P = 12.36 \text{ GPa}$  are  $\Delta_a = 0.423$  and  $\Delta_b = -0.314$ , with associated hopping amplitudes

$$\begin{aligned} t^z &= \begin{bmatrix} -0.334 & -0.177 \\ +0.177 & +0.212 \end{bmatrix}, \\ t^y &= \begin{bmatrix} -0.024 & 0.000 \\ 0.000 & +0.216 \end{bmatrix}, \\ t^{z+y} = t^{z-y} &= \begin{bmatrix} +0.085 & +0.216 \\ -0.216 & +0.109 \end{bmatrix}, \\ t^{2z} &= \begin{bmatrix} -0.171 & -0.011 \\ +0.011 & +0.035 \end{bmatrix}, \\ t^{2z+y} = t^{2z-y} &= \begin{bmatrix} 0.000 & +0.042 \\ -0.042 & -0.044 \end{bmatrix}. \end{aligned} \quad (3)$$

Figures 2(a) and 2(b) show the single-particle spectrum, calculated to illustrate the band structure at both  $P = 0.0$  and 12.36 GPa using all the hoppings in Eqs. (2) and (3) (“long-range hoppings”). In Figs. 3(a) and 3(b), similar results are presented but using only hoppings up to nearest-neighbor rungs (“short-range hoppings”). The band structures in both cases are similar. However, some discrepancies occur. For instance, at the edges, such as  $k_z = 0$  and  $\pi$ , the short-range hoppings present degeneracies (or near degeneracies) that are split in the long-range case. It is unclear if these details are significant or not, and without performing the DMRG calculations in both cases explicitly this issue cannot be answered conclusively. Here, we simply wish to alert the readers of these small differences for completeness.

The electronic interaction portion of the Hamiltonian

$$\begin{aligned} H_{\text{int}} &= U \sum_{i\gamma} n_{i\uparrow\gamma} n_{i\downarrow\gamma} + \left( U' - \frac{J}{2} \right) \sum_{\substack{i \\ \gamma < \gamma'}} n_{i\gamma} n_{i\gamma'} \\ &\quad - 2J \sum_{\substack{i \\ \gamma < \gamma'}} \mathbf{S}_{i\gamma} \cdot \mathbf{S}_{i\gamma'} + J \sum_{\substack{i \\ \gamma < \gamma'}} (P_{i\gamma}^{\dagger} P_{i\gamma'} + \text{H.c.}) \end{aligned} \quad (4)$$

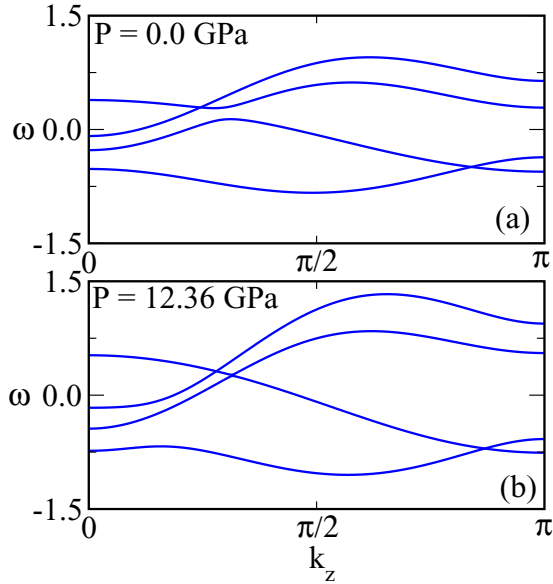


FIG. 2. Tight-binding band structure ( $U/W = 0.0$ ) involving hoppings up to the next-nearest neighbor rungs (i.e., long-range hoppings) for pressures of (a) 0.0 and (b) 12.36 GPa. The chemical potential is at zero energy for half-filling.

contains the standard intraorbital Hubbard repulsion  $U$  and the Hund's coupling  $J$ . The operator  $\mathbf{S}_{i\gamma}$  ( $n_{i\gamma}$ ) is the total spin (electronic density) for orbital  $\gamma$  at site  $i$ .  $P_{i\gamma}^\dagger$  ( $P_{i\gamma}$ ) are the pair creation (annihilation) operators. The standard relation  $U' = U - 2J$  is assumed. The operators are defined in terms of the creation and annihilation fermion operators as

$$\mathbf{S}_{i\gamma} = \sum_{\sigma\sigma'} c_{i\sigma\gamma}^\dagger \sigma_{\sigma\sigma'} c_{i\sigma'\gamma}, \quad (5)$$

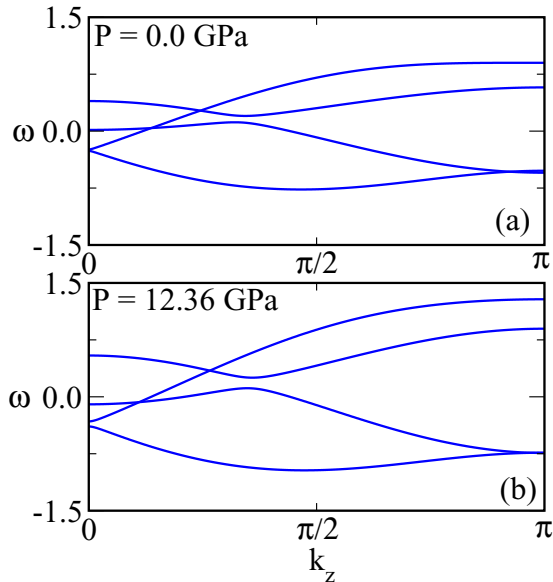


FIG. 3. Tight-binding band structure ( $U/W = 0.0$ ) involving hoppings only up to the nearest-neighbor rungs (i.e., short-range hoppings) for pressures of (a) 0.0 and (b) 12.36 GPa. The chemical potential is at zero energy for half-filling.

$n_{i\sigma\gamma} = c_{i\sigma\gamma}^\dagger c_{i\sigma\gamma}$ , and  $P_{i\gamma} = c_{i\downarrow\gamma} c_{i\uparrow\gamma}$ . The half-filling electronic density corresponds to two electrons per site.

We use the ground-state density matrix renormalization group (DMRG) technique with open boundary conditions in order to study the  $\text{BaFe}_2\text{S}_3$  ladder using the two-orbital Hubbard model previously defined. DMRG grows the lattice by adding sites in a “snakelike” geometry. We have studied in detail a ladder size of  $8 \times 2$  with up to four holes doped over a half-filled system. Calculations involving  $12 \times 2$  and  $16 \times 2$  ladders are also presented at half-filling. Keeping up to 800 states, the typical value of the discarded weight (truncation error) is of the order of  $10^{-5}$  for the doping cases studied. Within this level of error observables are converged. For the two-holes case, we can reach a similar accuracy only for  $8 \times 2$  ladders, and for this reason our study of binding energies is restricted to those ladders. With typical computer resources,  $8 \times 2$  ladder simulations with  $m = 800$  states require 3–4 days at half-filling. The two holes doped case needs more than a week, even if using only short-range hoppings. The use of the long-range hoppings substantially increases the time required for convergence. This is because of three different reasons. First, the most time consuming part of the DMRG process is computing the Hamiltonian connections, and with long-range hoppings one has to sum a large number of terms in the Hamiltonian. Second, at fixed on-site interactions ( $U$  and  $J$ ) and fixed density, the difficulty of the DMRG scales exponentially with the number of connections between system and environment, when a lattice is split in the middle. Third, our on-site Hilbert space is large due to the presence of two orbitals. In fact, the system we have studied can be translated into a one-dimensional one-orbital Hubbard model with hoppings up to 12th neighbors. This illustrates the substantial numerical effort presented here at the limit of what can be done with modern many-body computational techniques. We also want to remark that perhaps more modern versions of DMRG, such as those involving matrix product operators, may alleviate the effort needed in the present problem. In fact, recently,  $S = 1/2$  ladders including dipolar interactions were studied with up to 400 rungs with this method [37].

We will present a variety of charge and magnetic observables for doping of up to four holes on the half-filled system. The average occupation number of each orbital is

$$\langle n_\gamma \rangle = \frac{1}{N} \sum_{i,\sigma} \langle n_{i\sigma\gamma} \rangle. \quad (6)$$

We also calculate the spin-spin correlations by using the Fourier transform of the real space  $\langle \mathbf{S}_i \cdot \mathbf{S}_j \rangle$ ,

$$S(k_z, k_y) = \frac{1}{N^2} \sum_{i,j} e^{-i\vec{k} \cdot \vec{r}_{ij}} \langle \mathbf{S}_i \cdot \mathbf{S}_j \rangle, \quad (7)$$

where  $\mathbf{S}_i = \sum_\gamma \mathbf{S}_{i\gamma}$  (sum over the orbitals). Below, this spin structure factor will carry a subindex “L” or “S” depending on whether in the Hamiltonian the long-range or short-range hoppings are used, respectively.

To explore pairing tendencies, we study the binding energy of a pair of holes defined as [38]

$$\Delta E = E(N-2) + E(N) - 2E(N-1), \quad (8)$$

where  $E(M)$  is the ground-state energy of the model with a total of  $M$  electrons ( $M = N$  is half-filling). If the particles minimize their energy by creating a bound state then  $\Delta E$  is negative; if the holes become two independent particles, this corresponds to zero binding energy in the bulk limit. In the case where the particles do not bind, this quantity is positive for finite systems.

To study the effects of holes on the magnetic correlations, we define a projector  $P_{h\gamma}(i)$  at site  $i$  such that it projects out the portion of the ground state in which site  $i$  and orbital  $\gamma$  is occupied [39]:

$$P_{h\gamma}(i) = c_{i\downarrow\gamma}^\dagger c_{i\downarrow\gamma} c_{i\uparrow\gamma}^\dagger c_{i\uparrow\gamma}. \quad (9)$$

In order to work in the Hilbert space corresponding to  $N_h$  number of holes at specific locations, we apply a product of projectors onto the ground state with  $N_h$  holes,  $P_{h\gamma} = P_{h\gamma}(i_1)P_{h\gamma}(i_2)\dots P_{h\gamma}(i_{N_h})$ , where  $i$  is the site to be projected while respecting the fermionic normal ordering ( $i_i < i_2 < \dots < i_{N_h}$ ). For example,  $P_{ha} = P_{ha}(6)P_{ha}(8)$  projects out the occupied part of the ground state on orbital  $a$  at sites 6 and 8. In fact, for most results shown below, we only apply the projector onto orbital  $a$  in order to observe the corresponding local spin-spin correlations  $\langle \psi | \mathbf{S}_{ia} \cdot \mathbf{S}_{ja} P_{ha} | \psi \rangle / \langle \psi | P_{ha} | \psi \rangle$ , where the maximum possible magnitude of the correlations is  $3/4$ .

#### IV. RESULTS

This section presents our main results. We start with the half-filled case that should be contrasted with the experimental data for the two-leg  $\text{BaFe}_2\text{S}_3$  at pressures where magnetic order was reported. *The magnetic order observed experimentally emerges very clearly from our calculations.* We then proceed to the addition of holes, under the assumption that the high pressure used experimentally moves bands around in such a manner that the two-leg ladders become effectively doped. Our main result is that indications of pairing are found in small systems, opening the possibility that indeed superconducting tendencies may be present in the models studied here.

##### A. Half-Filling

Figure 4(a) shows the electronic population of the two orbitals calculated via DMRG as a function of  $U/W$ , for the two electrons per site half-filling case. Because of the crystal field splitting that locates orbital  $b$  approximately 0.7 eV below orbital  $a$ , in the weak coupling regime orbital  $b$  is considerably more populated. As the energy penalization for double occupancy increases with increasing  $U/W$ , eventually at  $U/W \sim 1$  both orbitals become effectively singly occupied. These orbital populations are robust varying the lattice size and also using either the “short” or “long” version of the hopping amplitudes, as shown in Fig. 4(a).

Figure 4(b) presents the spin structure factor at various wave vectors as a function of  $U/W$ . The wave vector  $(\pi, 0)$  clearly dominates, particularly in the regime of intermediate and strong coupling.  $S_S(\pi, 0)$  (see definition in caption of Fig. 4) starts growing already at  $U/W \simeq 0.4$  even before the full moments are developed, an intermediate coupling regime that several investigations assign to the iron based superconductors [6]. Once again, these results are robust

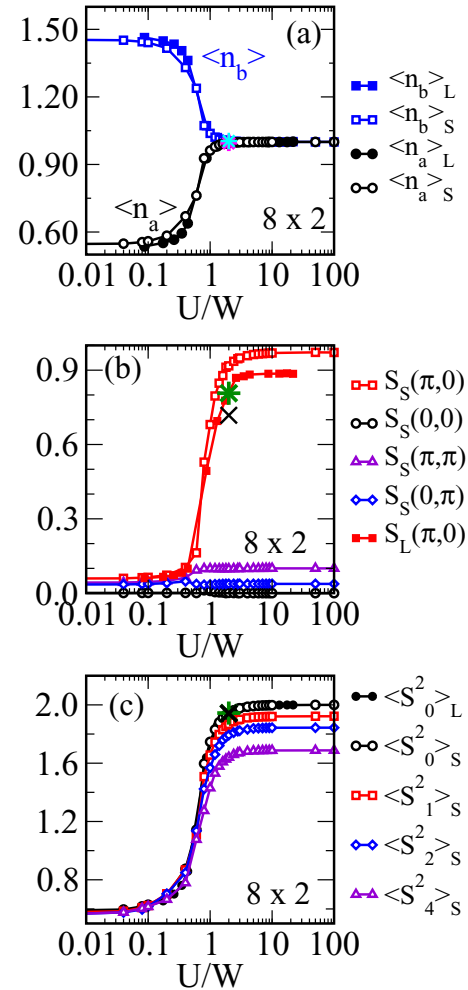


FIG. 4. Charge and magnetic properties of a half-filled  $8 \times 2$  ladder at  $P = 12.36$  GPa [Eq. (3)] studied with DMRG. Full (empty) points with subscript “L” (“S”) correspond to using long-range (short-range) hoppings. All results are at  $J/U = 0.25$ . (a) Average orbital occupation vs  $U/W$ . Black (blue) color is for orbital  $a$  ( $b$ ). The stars at  $U/W = 2.0$  indicate results using a  $12 \times 2$  lattice [cyan (magenta) for orbital  $b$  (a)]. Very similar results were obtained for a  $16 \times 2$  lattice (not shown). (b) Fourier transform of the spin-spin correlations (i.e., spin structure factor) at representative wave vectors, indicating the dominance of  $(\pi, 0)$  (see text). At  $U/W = 2.0$ ,  $S_S(\pi, 0)$  was also calculated using  $12 \times 2$  (green star) and  $16 \times 2$  (black X) lattices.  $S_S(\pi, 0)$  slightly decreases with system size because the one-dimensional nature of the lattice prevents long-range magnetic order. (c)  $\langle S^2 \rangle$  vs  $U/W$ , averaged over all sites. The subindexes 0, 1, 2, and 4 are the number of holes away from half-filling. The green star and black X are as in (b), suggesting small size effects. The convergence to 2 with increasing  $U/W$  at half-filling denotes a convergence to spin  $S = 1$ , as expected because  $J$  increases proportional to  $U$ .  $\langle S^2 \rangle$  slightly decreases with increasing number of holes because of dilution effects.

increasing the lattice size and using either “short” or “long” hopping amplitudes. The small decrease of  $S_S(\pi, 0)$  in Fig. 4(b) with increasing clusters from  $8 \times 2$  to  $16 \times 2$  is reasonable because a true long-range order is not expected in one dimension, but a slow power-law decay should instead prevail.

The dominance of the  $(\pi,0)$  magnetic order is in excellent agreement with neutron experiments for  $\text{BaFe}_2\text{S}_3$  [26]. In our model, this magnetic order dominance arises primarily from the comparable strength of the hopping amplitudes  $t^{y+z}$  along the diagonal of the elementary plaquettes contrasted with those along the nearest-neighbor sites along the rungs and legs. This comparable strength originates in the location of sulfur, that acts as a bridge between irons, up and down the middle of the ladder plaquettes. This is also the same reason for the dominance of the (degenerate)  $(\pi,0)$  and  $(0,\pi)$  wave vectors in planar geometries, at intermediate and strong couplings.

In two-leg ladders, the explicit breaking of the lattice rotational invariance renders  $(\pi,0)$  and  $(0,\pi)$  no longer degenerate. However, why  $(\pi,0)$  dominates over  $(0,\pi)$  according to the DMRG calculations? A possible simple explanation is the following. Consider a classical  $J_1$ - $J_2$  spin model for spins of magnitude 1, where  $J_1$  is the antiferromagnetic Heisenberg coupling for nearest-neighbors spins both along the rungs and legs, while  $J_2$  is the antiferromagnetic coupling along the plaquette diagonals. The energy of the  $(\pi,0)$  state is always smaller than the energy of the  $(0,\pi)$  because in  $(\pi,0)$  each spin always has two nearest-neighbor AFM links, while in  $(0,\pi)$  there is only one nearest-neighbor AFM link. While at small  $J_2/J_1$  the  $(\pi,\pi)$  order dominates as expected, a level crossing to  $(\pi,0)$  eventually occurs at  $J_2/J_1 = 0.5$ . This also provides a possible rationale for why  $(\pi,\pi)$  rather than  $(0,\pi)$  appears to be the subdominant order in Fig. 4(b): in these two-orbital Hubbard models for two-leg ladder materials, the ratio  $J_2/J_1$  between the effective Heisenberg couplings in strong coupling must be between 0.5 and 1.0.

Figure 4(c) plots the spin squared expectation value as a function of  $U/W$ , showing the formation of local moments. The upturn with increasing  $U/W$  occurs at values similar to those where  $S(\pi,0)$  starts growing. Eventually, at strong coupling,  $U/W > 1$ , the spins are fully developed and they acquire their maximum value  $S = 1$ , i.e., a magnetic moment  $2.0 \mu_B$ . Neutron scattering experiments at ambient pressure [26] report a moment of  $1.2 \mu_B$  ( $S \sim 0.6$ ), which we find at  $U/W \simeq 0.5$ ; first principles predict a value of  $2.0 \mu_B$  ( $S \sim 1.0$ ) at the same pressure [34]. Note that neutron scattering may be capturing a moment that is time averaged, thus reducing its value, and other techniques should be used to find the actual instantaneous spin [9,10]. Also note that comparing magnetic moment results of a two-orbital model versus calculations and experiments involving five orbitals is difficult. Regardless, intermediate to strong coupling is the physically relevant regime in this model from the magnetic moment perspective.

### B. One hole doped

Figure 5 shows results for the case of one hole doped into the half-filled system. Panel (a) displays the population of each orbital. As at half-filling, the crystal field splitting induces a large difference at weak coupling between the two orbitals. However, it is curious to observe that in the strong coupling regime the hole is still almost entirely located at orbital  $a$ , in spite of the presence of a gap induced by the repulsion  $U$ . Nevertheless, since the  $U$  is the same for both orbitals, the only asymmetry between the orbitals is the original crystal

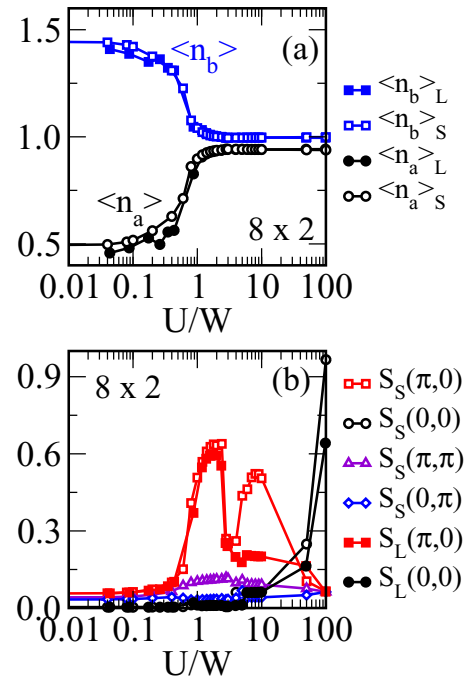


FIG. 5. Charge and magnetic properties of an  $8 \times 2$  ladder doped with one hole, at  $P = 12.36$  GPa [Eq. (3)] and studied with DMRG. Full (empty) points with subscript “L” (“S”) correspond to using long-range (short-range) hoppings. All results are at  $J/U = 0.25$ . (a) Average orbital occupancy vs  $U/W$ . Black (blue) color is for orbital  $a$  ( $b$ ). At small  $U/W$ , the crystal field creates a substantial difference in the populations. At large  $U/W$ , the  $b$  orbital converges approximately to one electron/site, while the  $a$  orbital contains most of the doped hole. The results are approximately the same for L and S hoppings. (b) Fourier transform of the spin-spin correlations (i.e., spin structure factor) at various representative wave vectors, indicating the dominance of  $(\pi,0)$ . At very large  $U/W$ , the one hole state becomes ferromagnetic due to double exchange tendencies, as discussed in the text.

field splitting that, therefore, must be inducing the asymmetric population with holes of the  $a$  orbital.

This strong-coupling Wannier orbital population, where one orbital is locked at one electron/site and the other at less than one electron/site, corresponds to an orbital selective Mott phase (OSMP) [40]. In this context, orbital  $b$  provides localized spins  $S = 1/2$ , that are in interaction with delocalized carriers at orbital  $a$ . The physics of the OSMP state suggests that this state, if realized in the present two-leg ladders, may have exotic transport properties that include a very small quasiparticle weight.

Panel (b) contains the spin structure factor. As in the case of half-filling, clearly the wave vector  $(\pi,0)$  dominates starting at  $U/W \sim 0.4$ , and irrespective of using “short”- or “long”-range hoppings. The dip at  $U/W \sim 3$  is unexpected and it may reflect on how the hole scrambles the original magnetic order as the size of the spin distortion around the hole changes with  $U/W$ . This spin scrambling effect can be better visualized in Fig. 6 where from the entire wave function of the one-hole state, a projection is made for the case where the hole is located at the sites indicated. While far from the projected hole the spin order is basically unchanged from the half-filled  $(\pi,0)$  pattern, in the

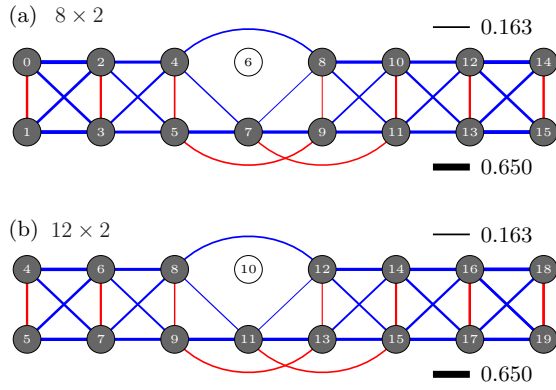


FIG. 6. Results obtained from the wave function of a dynamical hole at  $P = 12.36$  GPa [Eq. (3)], using  $U/W = 2$  and  $J/U = 0.25$ , for the case when the hole is projected on orbital  $a$  at the location denoted by the white circles [see Eq. (9)]. (a) Results for the  $8 \times 2$  lattice and (b) are for the  $12 \times 2$  lattice, showing that size effects are small. The thickness of the lines is linearly proportional to the magnitude of the spin-spin correlations involving orbital  $a$ . These correlations between spins at sites  $m$  and  $j$  are defined as  $\langle \psi | \mathbf{S}_{ma} \cdot \mathbf{S}_{ja} P_{ha}(i) | \psi \rangle / \langle \psi | P_{ha}(i) | \psi \rangle$ , where  $P_{ha}(i)$  was defined in the text. Blue denotes antiferromagnetic correlation while red is ferromagnetic. In (a),  $i = 6$ , and in (b),  $i = 10$ . Magnetic correlations away from the hole are very similar to those in the undoped case. In both (a) and (b), in the vicinity of the hole, a weak antiferromagnetic correlation between spins “across the hole” location can be clearly observed. For a discussion see the text.

vicinity of the hole there is an inevitable scrambling effect that broadens the  $(\pi, 0)$  peak. This shift of weight away from  $\pi$  along the leg direction is exemplified by the antiferromagnetic coupling “across the hole” involving, e.g., spins 4 and 8 on the  $8 \times 2$  lattice that otherwise should be ferromagnetically coupled. The  $12 \times 2$  results in the same panel indicate very small size effects. This across-the-hole AFM coupling has been observed in the  $t$ - $J$  model context before [41–43], and it is considered a precursor of spin-charge separation at least at short distances. In fact, the exact ground state of the  $U = \infty$  one-orbital Hubbard model in one dimension presents an exact decoupling between spin and charge with AFM couplings across all holes [44].

We warn the readers that there are some qualitative differences between the cases of short- and long-range hoppings. Of instance in Fig. 5(b)  $S_S(\pi, 0)$  has a “second peak” at  $U/W \sim 10$ , which is suppressed in  $S_L(\pi, 0)$ . We do not know the qualitative reasons for this difference. However, in the important region of pair binding  $U/W \sim 2$ , to be described later in the text, both short- and long-range hoppings give very similar results.

An interesting observation from Fig. 5(b) is that at very large  $U/W$  eventually the one hole state becomes ferromagnetic since  $S(0, 0)$  dominates. In multiorbital systems, especially in cases where some degrees of freedom are localized and others itinerant as it occurs in this model, double exchange mechanisms can favor ferromagnetic tendencies as it occurs in manganites [45]. In the large  $U/W$  regime, the effective Heisenberg couplings  $J_1$  and  $J_2$  are very small since they are inversely proportional to  $U$ , while the Hund coupling

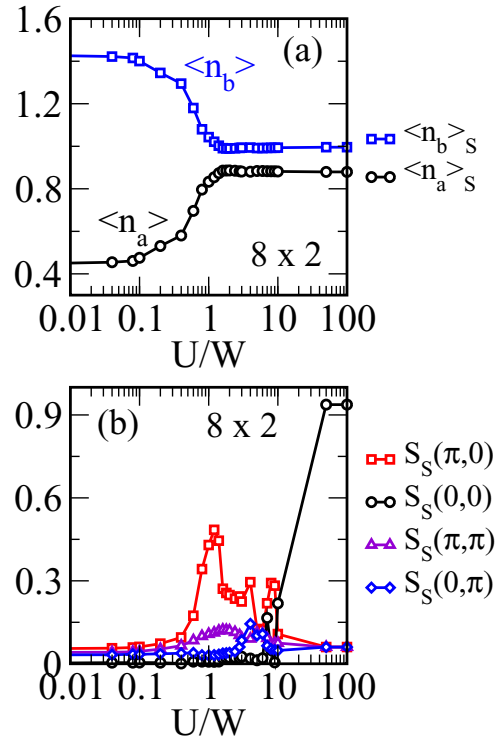


FIG. 7. Charge and magnetic properties of an  $8 \times 2$  ladder doped with two holes, at  $P = 12.36$  GPa [Eq. (3)], using short-range (“S”) hoppings, and studied with DMRG. All results are at  $J/U = 0.25$ . (a) Average orbital occupancy vs  $U/W$ . Black color is for orbital  $a$  and blue for orbital  $b$ . At small  $U/W$ , the crystal field creates a substantial difference in the populations. At large  $U/W$ , the  $b$  orbital converges approximately to one electron/site, while the  $a$  orbital contains most of the doped holes. (b) Fourier transform of the spin-spin correlations (i.e., spin structure factor) at representative wave vectors, indicating the dominance of  $(\pi, 0)$  at intermediate/large  $U/W$ . At very large  $U/W > 10$ , the two holes state becomes ferromagnetic due to double exchange tendencies, as discussed in the text and as for one hole.

being fixed to  $J/U = 0.25$  is very large. Such a regime is clearly favorable for double exchange tendencies, as shown by the DMRG results. This also indicates that ferromagnetic states are close in parameter space to the realistic regimes for iron superconductors, a conclusion that also emerged from previous investigations [21,24,25].

### C. Two holes doped

The results for two doped holes shown in Fig. 7 continue the trends observed before for one hole. Panel (a) shows the Wannier orbital populations as a function of  $U/W$ . As for one hole, at large  $U/W$  the orbital  $b$  population remains locked at one electron/site, while the two holes almost entirely reside at orbital  $a$ . This confirms the tendency towards an OSMP state with doping. With regards to the spin magnetic order, panel (b), the  $(\pi, 0)$  order still dominates in the broad region between  $U/W = 0.4$  and 10, but the spin order scrambling caused by the mobile holes reduces the intensity of  $S(\pi, 0)$  as expected. In addition, the tendency towards ferromagnetism triggered by double exchange continues at very large  $U/W$ .

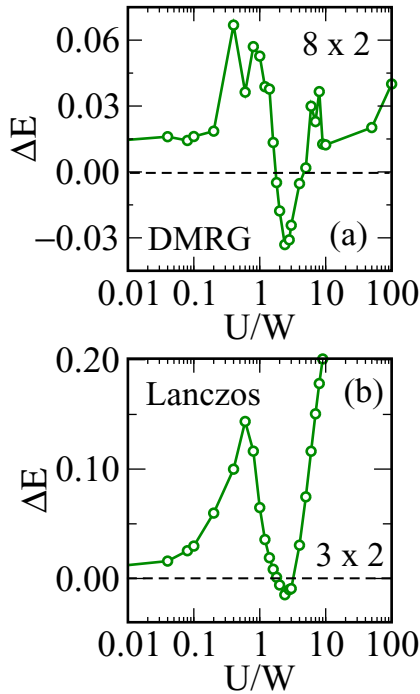


FIG. 8. Binding energy vs  $U/W$  calculated using (a) DMRG for an  $8 \times 2$  ladder and (b) Lanczos for a  $3 \times 2$  ladder. In both cases, we observe a nonmonotonic up-down-up behavior where the minimum of the binding energy can be found at  $U/W \sim 2$ . Since this minimum of  $\Delta E$  is negative, panel (a) suggests binding of holes between  $U/W \sim 1.5$  and  $U/W \sim 4.5$ . The results in both panels were obtained at  $P = 12.36$  GPa [Eq. (3)], using short-range hoppings, and  $J/U = 0.25$ .

#### D. Binding energy

After calculating the ground-state energies for the  $N$ ,  $N - 1$  (1 hole), and  $N - 2$  (2 holes) subspaces, we can also calculate the binding energy  $\Delta E$  previously defined. The remarkable result shown in Fig. 8(a) is that for the  $8 \times 2$  cluster this quantity becomes negative between  $U/W \sim 1.5$  and  $U/W \sim 4.5$ . This is a broad region, in spite of the perceived narrowness in panel (a) because of the logarithmic scale used. In this regime, the spins are already well developed and near saturation as it was shown in Fig. 4(c). Considering that holes are located at orbital  $a$ , this surprising result brings similarities with negative binding energies found in one-orbital models for the cuprates, such as the  $t$ - $J$  [38]. In fact, the crude rationale for binding based on the “number of broken AFM links” may apply here as well [38]. In this context, binding occurs because each hole damages the AFM spin state, and the manner to minimize the size of that distorted magnetic background is by bringing the holes together. It is also interesting that exact results obtained via the Lanczos method applied to a very small  $3 \times 2$  lattice produce a profile for the binding energy, shown in Fig. 8(b), that qualitatively resembles panel (a) suggesting that size effects are mild. Alas, as already explained, we have not been able to reach sufficient accuracy in the two holes sector to confirm the pairing tendencies of Fig. 8(a) with larger lattices, thus our pairing analysis below is restricted to the  $8 \times 2$  cluster.

The results in panel (a) suggesting pairing in a region of parameter space brings analogies with the negative binding

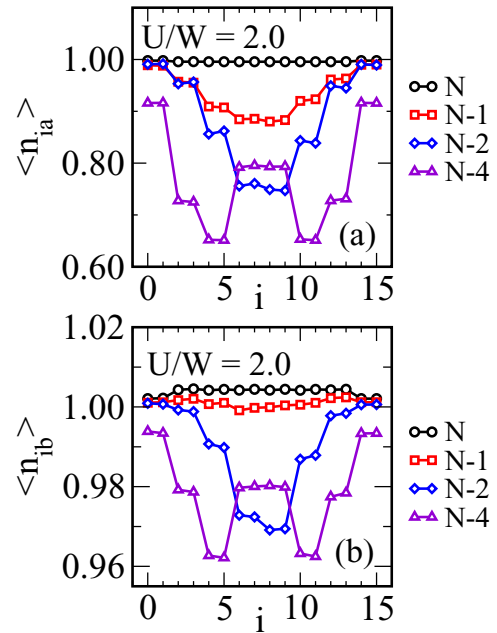


FIG. 9. Real space electronic density of each orbital [panel (a) is for orbital  $a$ , while panel (b) for orbital  $b$ ] using an  $8 \times 2$  ladder,  $U/W = 2.0$ ,  $J/U = 0.25$ , short-range hoppings, and at  $P = 12.36$  GPa [Eq. (3)]. Results are shown for half-filling ( $N$  electrons), one hole ( $N - 1$ ), two holes ( $N - 2$ ), and four holes ( $N - 4$ ) as a function of the position “ $i$ ” [see Fig. 6(a) for the site labeling convention]. The most striking result corresponds to four holes where the presence of two minima is indicative of hole pairing. Doping of four holes reduces the orbital  $a$  electron density by approximately 25%, while orbital  $b$  has a charge depletion of only  $\sim 3\%$ , illustrating again that holes mainly reside at orbital  $a$ .

energies reported before in Kondo lattice models for heavy fermions [46]. For instance, in Fig. 2(b) of Ref. [46], a negative  $\Delta E$  is reported using up to  $32 \times 2$  lattices. Even the pair-pair correlation functions of Fig. 3(b) of Ref. [46] (unfortunately not within the reach of the present study that uses the full two-orbital Hubbard model) suggest a dominant pairing tendency in the doped Kondo lattice on two-leg ladders. Perhaps having holes primarily at orbital  $a$  (as shown before), while orbital  $b$  remains singly occupied at strong coupling, effectively transforms our model into a Kondo lattice model.

To further test the pairing implication of finding a negative binding energy in Fig. 8, we have also analyzed the real space distribution of holes in the doped system. In Fig. 9(a), the electronic density is shown for orbital  $a$ , where the holes are mostly located, for each of the 16 sites of the  $8 \times 2$  lattice at coupling  $U/W = 2$  where  $\Delta E$  is negative. For  $N$  electrons, i.e., half-filled, the electronic density is basically uniform. In the case of  $N - 1$  electrons, i.e., one hole, this hole is located in the middle of the cluster as expected for a system with open boundary conditions. For the case of two holes corresponding to  $N - 2$  electrons, these two holes are also located near the center of the cluster but in a tight manner compatible with pairing. The most important result is for the case of four holes, corresponding to  $N - 4$  electrons, since Fig. 9(a) indicates the presence of *two* minima in the electronic density, a result compatible with the presence of two hole pairs, as opposed

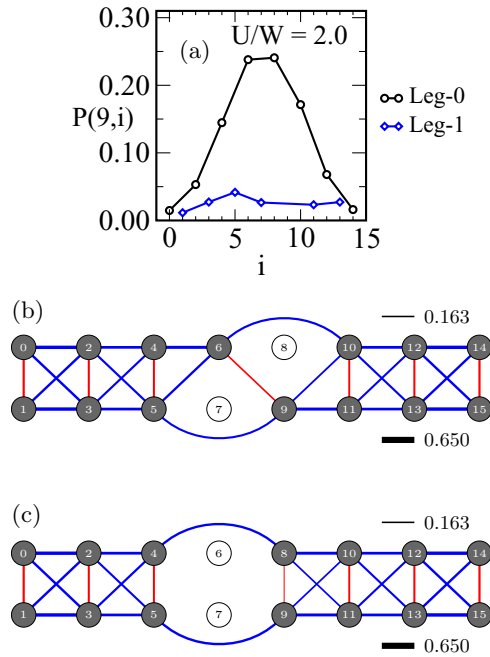


FIG. 10. (a) For the case of the two holes ground state on an  $8 \times 2$  ladder, this panel shows the probability of a hole to be located at a site “ $i$ ” assuming the other hole is fixed at site 9 of the bottom leg (Leg-1). Results are normalized to one. Since sites are labeled with a snakelike geometry where site zero starts from the upper leg (Leg-0), this panel indicates that the two holes in the bound state are primarily located in different legs. See Fig. 6(a) for site labeling details. (b) and (c) Results from the DMRG ground state wave function of two holes on an  $8 \times 2$  cluster, using  $U/W = 2.0$  (binding region) and  $J/U = 0.25$ , and with short-range hoppings at  $P = 12.36$  GPa [Eq. (3)]. Shown are spin-spin correlations for the case where the two holes are projected to be at the white circles, i.e., (b) along a plaquette diagonal and (c) along a rung. These are the two most dominant configurations in the hole pair. The spin-spin magnetic correlations are defined as  $\langle \psi | \mathbf{S}_{ma} \cdot \mathbf{S}_{na} P_{ha}(i) P_{ha}(j) | \psi \rangle / \langle \psi | P_{ha}(i) P_{ha}(j) | \psi \rangle$ , involving only orbital  $a$  because it is the primary location for the doped holes. In (b),  $i = 7$  and  $j = 8$  and in (c),  $i = 6$  and  $j = 7$ . Blue (red) lines are AFM (FM) bonds. For all hole configurations, the  $(\pi, 0)$  magnetic order is substantially distorted only near the holes. Note also the presence of “across the hole” AFM correlations in both panels.

to a single broad minimum which would indicate independent holes or four minima which would signal a charge density wave of holes. There are also no indications of phase separation. The results in Fig. 9(b) for orbital  $b$  simply mirror those of orbital  $a$  but with a far more suppressed hole density.

Figure 10(a) illustrates the internal structure of the hole pairs that we have found using the  $8 \times 2$  cluster. This figure is based on the wave function of two holes, with one of the holes projected to site “9,” which is on “Leg-1”. This panel shows that the second hole is primarily located on the other leg, i.e., “Leg-0”, mainly at the sites either in the same rung as “9” or diagonally across the plaquettes. Projecting now the two holes to those particular locations, these two dominant “plaquette diagonal” and “rung” states for the pair of holes are shown in Figs. 10(b) and 10(c), respectively. Similarly, as for the case of one hole, there is a notorious “across the hole” antiferromagnetic coupling between spins that otherwise

should be ferromagnetically coupled in the undoped system. This AFM correlation facilitates the movement of the hole. Note also that if in panel (b) the hole located at “8” and the spin at “6” are interchanged, as it would happen via the action of electronic hopping and assuming that the AFM and FM bonds remain the same as if they were elastic bands, then panel (c) is obtained. In fact, this panel (c) has an AFM across-the-hole coupling between “4” and “8” and a FM coupling between “8” and “9” that was originally a FM coupling along the diagonal from “6” to “9” in panel (b). Then panels (b) and (c) are compatible with one another with regards to hole pairing: the two holes are oscillating in different legs close to one another due to an attraction created by the antiferromagnetic background.

## V. CONCLUSIONS

In this publication, we have presented the first study of a realistic (derived from first principles) electronic model Hamiltonian for the two-leg ladder compound  $\text{BaFe}_2\text{S}_3$  that was recently shown to become superconducting at high pressure [26,27]. The model has two orbitals and electronic hoppings beyond nearest-neighbor iron sites, rendering its study difficult even with the powerful DMRG method. For this reason, our analysis has been restricted to relatively small clusters. Nevertheless, we have been able to extract interesting information from the model that is in good agreement with experiments. For example, the parent compound has magnetic order involving ferromagnetic rungs that are coupled antiferromagnetically along the legs, as found in neutron scattering experiments [26]. In the strong coupling limit, this order emerges from the competition between antiferromagnetic Heisenberg couplings along rungs and legs and along the diagonals of the plaquettes. With hole doping, we observed that only one of the two Wannier orbitals used here becomes populated. This indicates a tendency towards effective models involving a combination of itinerant and localized orbitals, as in the context of an orbital selective Mott phase. Even more exciting, we have found that at strong coupling and using an  $8 \times 2$  cluster with two holes, there are indications of hole pair formation induced by antiferromagnetism. While this result must be confirmed using larger systems and more DMRG states, a challenging task, it suggests that this type of two-orbital models contains the essence of the mechanism for superconductivity in iron-based two-leg ladders, a mechanism that could be similar to that in layered systems. As a consequence, our present effort paves the way and motivates further studies in this context. We believe that the theoretical and experimental analysis of iron-based two-leg ladders may prove to be as interesting and illuminating as the early studies in copper oxide two-leg ladders were for cuprate physics, providing a novel playground in the context of iron-based high- $T_c$  superconductivity.

## ACKNOWLEDGMENTS

N.P., A.M., and E.D. were supported by the National Science Foundation Grant No. DMR-1404375. N.P. was also partially supported by the U.S. Department of Energy (DOE), Office of Basic Energy Science (BES), Materials Science and

Engineering Division. Part of this work was conducted at the Center for Nanophase Materials Sciences, sponsored by the Scientific User Facilities Division (SUFD), BES, DOE, under contract with UT-Battelle. A.N. and G.A. acknowledge support

by the Early Career Research program, SUFD, BES, DOE. Computer time was provided in part by resources supported by the University of Tennessee and Oak Ridge National Laboratory Joint Institute for Computational Sciences.

- 
- [1] D. C. Johnston, *Adv. Phys.* **59**, 803 (2010), and references therein.
- [2] G. R. Stewart, *Rev. Mod. Phys.* **83**, 1589 (2011).
- [3] P. J. Hirschfeld, M. M. Korshunov, and I. I. Mazin, *Rep. Prog. Phys.* **74**, 124508 (2011).
- [4] D. J. Scalapino, *Rev. Mod. Phys.* **84**, 1383 (2012).
- [5] A. V. Chubukov, *Annu. Rev. Condens. Matter Phys.* **3**, 57 (2012).
- [6] P. C. Dai, J. P. Hu, and E. Dagotto, *Nat. Phys.* **8**, 709 (2012), and references therein.
- [7] E. Dagotto, *Rev. Mod. Phys.* **85**, 849 (2013).
- [8] D. Liu, W. Zhang, D. Mou, J. He, Y. Ou, Q. Wang, Z. Li, L. Wang, L. Zhao, S. He *et al.*, *Nat. Commun.* **3**, 931 (2012).
- [9] F. Bondino, E. Magnano, M. Malvestuto, F. Parmigiani, M. A. McGuire, A. S. Sefat, B. C. Sales, R. Jin, D. Mandrus, E. W. Plummer, D. J. Singh, and N. Mannella, *Phys. Rev. Lett.* **101**, 267001 (2008).
- [10] H. Gretarsson, A. Lupascu, J. Kim, D. Casa, T. Gog, W. Wu, S. R. Julian, Z. J. Xu, J. S. Wen, G. D. Gu *et al.*, *Phys. Rev. B* **84**, 100509(R) (2011).
- [11] E. Dagotto, J. Riera, and D. Scalapino, *Phys. Rev. B* **45**, 5744(R) (1992).
- [12] E. Dagotto and T. M. Rice, *Science* **271**, 618 (1996).
- [13] E. Dagotto, *Rep. Prog. Phys.* **62**, 1525 (1999).
- [14] M. Uehara, T. Nagata, J. Akimitsu, H. Takahashi, N. Mori, and K. Kinoshita, *J. Phys. Soc. Jpn.* **65**, 2764 (1996).
- [15] J. M. Caron, J. R. Neilson, D. C. Miller, A. Llobet, and T. M. McQueen, *Phys. Rev. B* **84**, 180409(R) (2011).
- [16] H. Lei, H. Ryu, A. I. Frenkel, and C. Petrovic, *Phys. Rev. B* **84**, 214511 (2011).
- [17] B. Sapiro, S. Calder, B. Sipos, H. Cao, S. Chi, D. J. Singh, A. D. Christianson, M. D. Lumsden, and A. S. Sefat, *Phys. Rev. B* **84**, 245132 (2011).
- [18] Y. Nambu, K. Ohgushi, S. Suzuki, F. Du, M. Avdeev, Y. Uwatoko, K. Munakata, H. Fukazawa, S. Chi, Y. Ueda, and T. J. Sato, *Phys. Rev. B* **85**, 064413 (2012).
- [19] J. M. Caron, J. R. Neilson, D. C. Miller, K. Arpino, A. Llobet, and T. M. McQueen, *Phys. Rev. B* **85**, 180405(R) (2012).
- [20] F. Du, K. Ohgushi, Y. Nambu, T. Kawakami, M. Avdeev, Y. Hirata, Y. Watanabe, T. J. Sato, and Y. Ueda, *Phys. Rev. B* **85**, 214436 (2012).
- [21] Q. Luo, A. Nicholson, J. Rincón, S. Liang, J. Riera, G. Alvarez, L. Wang, W. Ku, G. D. Samolyuk, A. Moreo, and E. Dagotto, *Phys. Rev. B* **87**, 024404 (2013).
- [22] W. Lv, A. Moreo, and E. Dagotto, *Phys. Rev. B* **88**, 094508 (2013).
- [23] C. Monney, A. Uldry, K. J. Zhou, A. Krzton-Maziopa, E. Pomjakushina, V. N. Strocov, B. Delley, and T. Schmitt, *Phys. Rev. B* **88**, 165103 (2013).
- [24] Q. Luo and E. Dagotto, *Phys. Rev. B* **89**, 045115 (2014).
- [25] Q. Luo, K. Foyevtsova, G. D. Samolyuk, F. Reboredo, and E. Dagotto, *Phys. Rev. B* **90**, 035128 (2014).
- [26] H. Takahashi, A. Sugimoto, Y. Nambu, T. Yamauchi, Y. Hirata, T. Kawakami, M. Avdeev, K. Matsubayashi, F. Du, C. Kawashima, H. Soeda, S. Nakano, Y. Uwatoko, Y. Ueda, T. J. Sato, and K. Ohgushi, *Nat. Mater.* **14**, 1008 (2015).
- [27] T. Yamauchi, Y. Hirata, Y. Ueda, and K. Ohgushi, *Phys. Rev. Lett.* **115**, 246402 (2015).
- [28] S. R. White, *Phys. Rev. Lett.* **69**, 2863 (1992); U. Schollwöck, *Rev. Mod. Phys.* **77**, 259 (2005).
- [29] Y. Piskunov, D. Jérôme, P. Auban-Senzier, P. Wzietek, and A. Yakubovskiy, *Phys. Rev. B* **72**, 064512 (2005), and references therein.
- [30] R. Arita, H. Ikeda, S. Sakai, and M.-T. Suzuki, *Phys. Rev. B* **92**, 054515 (2015).
- [31] P. Giannozzi, S. Baroni, N. Bonini, M. Calandra, R. Car, C. Cavazzoni, D. Ceresoli, G. L. Chiarotti, M. Cococcioni, I. Dabo *et al.*, *J. Phys. Condens. Matter* **21**, 395502 (2009).
- [32] J. P. Perdew, K. Burke, and M. Ernzerhof, *Phys. Rev. Lett.* **77**, 3865 (1996).
- [33] Y. Hirata, S. Maki, J.-i. Yamaura, T. Yamauchi, and K. Ohgushi, *Phys. Rev. B* **92**, 205109 (2015).
- [34] For spin-density functional calculation, see M.-T. Suzuki, R. Arita, and H. Ikeda, *Phys. Rev. B* **92**, 085116 (2015).
- [35] A. A. Mostofi, J. R. Yates, Y.-S. Lee, I. Souza, D. Vanderbilt, and N. Marzari, *Comput. Phys. Commun.* **178**, 685 (2008).
- [36] I. Souza, N. Marzari, and D. Vanderbilt, *Phys. Rev. B* **65**, 035109 (2001).
- [37] S. R. Manmana, E. M. Stoudenmire, K. R. A. Hazzard, A. M. Rey, and A. V. Gorshkov, *Phys. Rev. B* **87**, 081106(R) (2013), and references therein.
- [38] E. Dagotto, *Rev. Mod. Phys.* **66**, 763 (1994), and references therein.
- [39] S. R. White and D. J. Scalapino, *Phys. Rev. B* **55**, 6504 (1997).
- [40] V. I. Anisimov, I. A. Nekrasov, D. E. Kondakov, T. M. Rice, and M. Sigrist, *Eur. Phys. J. B* **25**, 191 (2002); A. Liebsch, *Phys. Rev. B* **70**, 165103 (2004); A. Georges, L. de Medici, and J. Mravlje, *Annu. Rev. Condens. Matter Phys.* **4**, 137 (2013); J. Rincón, A. Moreo, G. Alvarez, and E. Dagotto, *Phys. Rev. Lett.* **112**, 106405 (2014), and references therein.
- [41] G. B. Martins, C. Gazza, J. C. Xavier, A. Feiguin, and E. Dagotto, *Phys. Rev. Lett.* **84**, 5844 (2000).
- [42] G. B. Martins, C. Gazza, and E. Dagotto, *Phys. Rev. B* **62**, 13926 (2000).
- [43] G. B. Martins, J. C. Xavier, C. Gazza, M. Vojta, and E. Dagotto, *Phys. Rev. B* **63**, 014414 (2000), and references therein.
- [44] M. Ogata and H. Shiba, *Phys. Rev. B* **41**, 2326 (1990).
- [45] E. Dagotto, T. Hotta, and A. Moreo, *Phys. Rep.* **344**, 1 (2001).
- [46] J. C. Xavier and E. Dagotto, *Phys. Rev. Lett.* **100**, 146403 (2008), and references therein.